Sequential Bayesian Methods for Resolution Enhancement of TIR Image Sequences

Paolo Addesso, Maurizio Longo *Member, IEEE*, Rocco Restaino *Member, IEEE*, Gemine Vivone

***Abstract*—The availability of remotely sensed image sequences characterized by both spatial and temporal high resolution is crucial in many applications, ranging from agriculture to Earth surface hazard monitoring. To date, image sequences presenting such desirable characteristics in both domains are not directly obtainable by a single device and thus a viable solution is represented by the joint use of multisensor information. In this work we propose a solution, based on Bayesian sequential estimation, for fusing two image sequences characterized by complementary features. Together with the assessment of two different sequential estimation approaches, a novel method for constructing a sharpened observations is here presented. The proposals are then evaluated by employing different datasets acquired by the SEVIRI and MODIS sensors, showing remarkable improvements with respect to classical approaches.**

***Index Terms*—Remote sensing, Land Surface Temperature, MAP Estimation, Thermal Image Enhancement, Sequential Bayesian Methods, Interacting Multiple Model**

I. Introduction

Accurate and frequent measures of *at-sensor Brightness Temperature* (*BT*) are required for remote sensing applications, such as wild fires or drought detection [8], [14], energy flux balances [7], [19], evaluation of soil moisture [28]. Therefore the relevant feature of the dataset is its spatial *and* temporal resolution.

Technological and computational constraints generally prohibit that sensors with high spatial accurateness collect data frequently enough, so that some sort of post-acquisition enhancement is in force. As far as sequences of thermal images are considered, proposed approaches for such enhancement exploit information contained in different parts of the spectrum [4], [19], [25], [27] or captured by cameras with different characteristics on the same scene. Thus, an *high spatial/high temporal* resolution is achieved by synthetic image sequences constructed by fusing the information coming from multiple sensors [12], [17].

Following this concept of data fusion, in this paper we employ a Bayesian framework already adopted in other Earth Observations applications, as Data Assimilation [15], [16], [35]. In particular, we consider *Bayesian sequential procedures* that take advantage from the correlation in image sequences [3]. In the latter work, by the same authors, the classical Kalman Filter (KF) [18] was employed, that however was unable to follow all the various dynamics exhibited by the BT during the day. To circumvent this difficulty, the concurrent operation of multiple different algorithms, together with an appropriate mixing criterion, could represent a viable solution. Several approaches of this class models have been presented in the literature [9], [21], [23]. A computationally efficient one is the *Interacting Multiple Model* (*IMM*) [10] that achieves the same performances of a second order multiple model with m hypothesis by running only m filters, instead of m^2. Preliminary results concerning the application of IMM to the enhancement of TIR image sequence enhancing has been presented in [1]. In the present paper we further elaborate on this approach, adjoining a method to enrich the information exploited at each step of the algorithm. In fact, one weakness of the straightforward application of the Bayesian filters is the failure to introduce an accurate modeling of the LR images in relation to the required HR sequence [11]. Actually, the simpler interpolation of the LR image to the HR resolution may yield better results than the Bayesian filters, as it allows also to incorporate an implicit description of the pixels spatial correlation [1]. However the practice of feeding the estimation algorithms with an enriched information is becoming common in many fields. Indeed, by learning lessons from the beneficial contribution that resolution enhanced images provide in visual interpretation by experts [20], sharpening algorithms have been used as a preliminary phase for many signal processing methodologies, as change detection [30] and object recognition [24]. In this work we investigate the possibility of constructing a more detailed observation than the mere LR current image by fusing it with details extracted from the last available HR image.

The performances of the proposed algorithms have been assessed on several datasets, employing both SEVIRI and MODIS acquisitions. The first has spatial resolution of about 6 km and acquisition interval of 15 min. The second, actually the concatenation of Terra and Aqua acquisitions, has spatial resolution of about 1 km and acquisition interval ranging from about 4 to about 8 hours. The validation is performed by exploiting two different protocols. According to the first one, only the SEVIRI sequence is employed. In particular the original images act as a reference HR datasets, while the needed LR sequence is obtained by degrading the original sequence to a lower resolution, allowing for any desired resolution ratio between HR and LR images; furthermore the complete availability of the HR images allows to freely select the instants at which they are fed to the estimation algorithms

P. Addesso, M. Longo, R. Restaino are with the Department of Information Eng., Electrical Eng. and Applied Math. (DIEM), University of Salerno, Via Giovanni Paolo II, 132 I-84084 Fisciano (SA), Italy. Phone: +39 089964350, Fax: +39 089964218. E-mails:{paddesso, longo, restaino}@unisa.it. G. Vivone is with North Atlantic Treaty Organization (NATO) Science and Technology Organization (STO) Centre for Maritime Research and Experimentation, I-19126 La Spezia, Italy. This work was partly performed under the provisions of IRRISAT Project, sponsored by Regione Campania (CUP: B35C11000090004)

and those at which sample outputs are computed. The second validation procedure constitutes the real data assessment of the proposals, in which, according to the cited specifications, the MODIS images plays the role of the HR information, while the set of SEVIRI images, at the nominal resolution, acts as the LR sequence. In this case, the validation is performed by supposing one available MODIS image to be unknown and then estimated through the developed algorithms.

Sect. II contains the mathematical formalization of the HR images estimation problem, based on the Bayesian framework. In particular the two selected approaches, based on KF and IMM are here presented. Sect. III illustrates the implementation details of the chosen methods for the application to the resolution enhancing of TIR image sequences. The validation of the approach is reported in Sect. IV, while Sect. V contains some final considerations and the further lines of research arising from this study.

II. Problem statement

The objective of this work is to construct a *high temporal resolution/High Spatial Resolution* (*htr/HSR*) sequence $\mathcal{E} = \{\mathbf{E}_k : k \in T_E\}$ of synthetic BTs by fusing a *low temporal resolution/High Spatial Resolution* (*ltr/HSR*) sequence $\mathcal{H} = \{\mathbf{H}_m : m \in T_H\}$ and a *high temporal resolution/Low Spatial Resolution* (*htr/LSR*) sequence $\mathcal{L} = \{\mathbf{L}_n : n \in T_L\}$.

We refer to the scenario depicted in Fig. 1, that is based on some simplifying assumptions. In particular we let the support of $\mathcal{E}$ coincide with that of $\mathcal{L}$, namely we set $T_E = T_L$ and choose the resolution of $\mathcal{H}$ as the target accuracy for $\mathcal{E}$. Although a more general setting can be conceived, this situation encompasses the typical requirements of practical applications. On the other hand, we adopt the further hypothesis that the domain of $\mathcal{H}$ is a subset of that of $\mathcal{E}$, namely $T_H \subset T_E = T_L$. The latter condition is hardly verified in real examples but will be kept, at the price of a passable approximation, to avoid cumbersome notations.

In this work we recast the inference of the unknown sequence $\mathcal{E}$ from the available data $\mathcal{H}$ and $\mathcal{L}$ within the *State-Space Model* (*SSM*) formalization [13], in which $\mathcal{E}$ constitutes the hidden state and $\mathcal{H}$ and $\mathcal{L}$ represents the accessible information. Accordingly, the time evolution of state and observation sequences is described through the couple of equations

$$\mathbf{x}_k = \mathbf{f}_k\left(\mathbf{x}_{k-1}\right) + \mathbf{w}_k, \tag{1}$$

$$\mathbf{y}_k = \mathbf{h}_k\left(\mathbf{x}_k\right) + \mathbf{n}_k \tag{2}$$

or, possibly, its linear version

$$\mathbf{x}_k = \mathbf{A}_k\mathbf{x}_{k-1} + \mathbf{w}_k, \tag{3}$$

$$\mathbf{y}_k = \mathbf{C}_k\mathbf{x}_k + \mathbf{n}_k. \tag{4}$$

Specifically, the state vector $\mathbf{x}_k$ is composed by the S pixels of image $\mathbf{E}_k$ arranged by columns through the operator $\mathrm{vec}\left(\cdot\right)$, i.e., $\mathbf{x}_k = \mathrm{vec}\left(\mathbf{E}_k\right) := \left[E_k\left(1\right), \ldots, E_k\left(S\right)\right]^T$ and of the process noise $\mathbf{w}_k$ (assumed independent zero mean Gaussian with covariance $\mathbf{Q}_k$). On the other side, the observation equation (2) models the relation of the available information at time k, represented by the observation vector $\mathbf{y}_k$, with the unobservable state $\mathbf{x}_k$, as represented by $\mathbf{h}_k\left(\mathbf{x}_k\right)$ and by the observation noise $\mathbf{n}_k$ (again assumed independent zero mean Gaussian with covariance $\mathbf{R}_k$).

A. Kalman Filter (KF)

The Markov hypothesis implied by the SSM formalization allows to find the optimal Bayesian estimation of the state $\mathbf{x}_k$, given the observations $\mathbf{y}_{0:k}$ until time k, by means of recursive procedures [33]. In the case of linear SSM the optimal recursion is represented by the *Kalman Filter* (*KF*) [18], that, due to the Gaussianity of all the involved distributions, consists in simply propagating the first two moments of the state posterior distribution. If $\widehat{\mathbf{x}}_{i|j}$ indicates the mean (and state estimate) at time i, given the observations until time j and $\mathbf{P}_{i|j}$ the corresponding covariance matrix, the KF is described by the following steps:

- *Initialization.* Set the initial value for the estimated state $\widehat{\mathbf{x}}_{0|0}$ and for the initial error covariance $\mathbf{P}_{0|0}$.
- *Propagation.* Compute the *a priori* estimates:

$$\widehat{\mathbf{x}}_{k|k-1} = \mathbf{A}_k\widehat{\mathbf{x}}_{k-1|k-1} \tag{5}$$

$$\mathbf{P}_{k|k-1} = \mathbf{A}_k\mathbf{P}_{k-1|k-1}\mathbf{A}_k^T + \mathbf{Q}_k \tag{6}$$

- *Update.* Calculate the *Kalman gain*

$$\mathbf{K}_k = \mathbf{P}_{k|k-1}\mathbf{C}_k^T\left(\mathbf{C}_k\mathbf{P}_{k|k-1}\mathbf{C}_k^T + \mathbf{R}_k\right)^{-1} \tag{7}$$

  and then compute the *a posteriori* estimates

$$\widehat{\mathbf{x}}_{k|k} = \widehat{\mathbf{x}}_{k|k-1} + \mathbf{K}_k\left(\mathbf{y}_k - \mathbf{C}_k\widehat{\mathbf{x}}_{k|k-1}\right) \tag{8}$$

$$\mathbf{P}_{k|k} = \left(\mathbf{I} - \mathbf{K}_k\mathbf{C}_k\right)\mathbf{P}_{k|k-1}, \tag{9}$$

  where $\mathbf{I}$ indicates the identity matrix of proper order.

Despite its simplicity, the KF shows remarkable performances also in the case of non-linear SSM through its generalization, named *Extended Kalman Filter* (*EKF*). It consists in employing Eqs. (5-9) after calculating the state-transition matrix $\mathbf{A}_k$ and the observation matrix $\mathbf{C}_k$ by linearizing Eqs. (1-2) around the available estimates, namely by the formulas

$$\mathbf{A}_k = \left.\frac{\partial}{\partial\mathbf{x}_{k-1}}\mathbf{f}_k\left(\mathbf{x}_{k-1}\right)\right|_{\mathbf{x}_{k-1}=\widehat{\mathbf{x}}_{k-1|k-1}}, \tag{10}$$

$$\mathbf{C}_k = \left.\frac{\partial}{\partial\mathbf{x}_k}\mathbf{h}_k\left(\mathbf{x}_k\right)\right|_{\mathbf{x}_k=\widehat{\mathbf{x}}_{k|k-1}}. \tag{11}$$

Furthermore, the propagation of the previous estimate $\widehat{\mathbf{x}}_{k-1|k-1}$ and the calculation of the predicted observation from $\widehat{\mathbf{x}}_{k|k-1}$ is computed through the nonlinear equations (1) and (2), respectively.

B. Interacting Multiple Model (IMM)

As stated before, a single model, hence a single KF, may not be able to capture all the diverse dynamics involved in the evolution of the states and observation sequences. To circumvent this difficulty, a possible solution is to run concurrently more than one KF, and to properly mix the corresponding estimates.

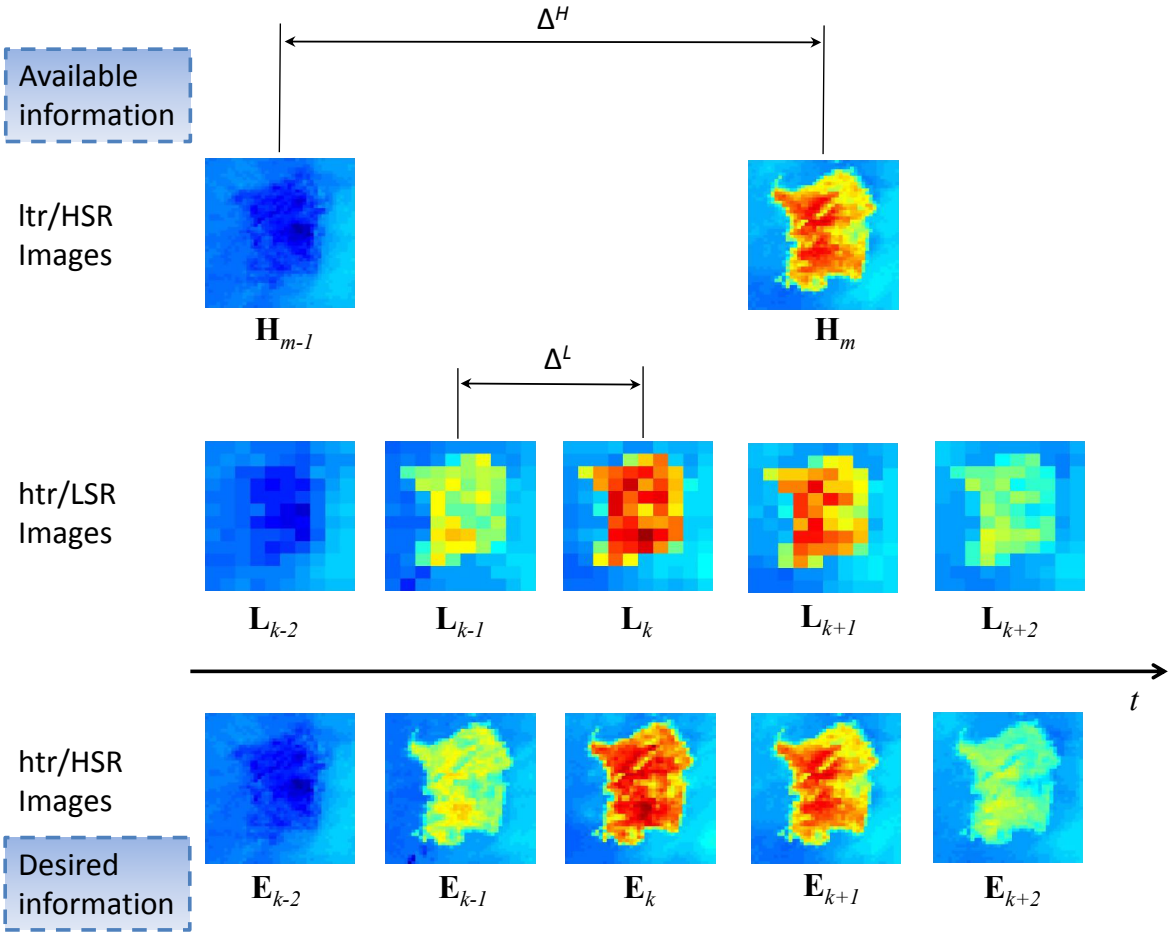

Fig. 1: Reference information timeline.

In the *Interacting Multiple Model* (*IMM*) [10] a Markov chain $M(k)$, characterized by the transition matrix

$$\begin{aligned}\mathbf{P} &= \{p_{ij}\}_{i,j=1,\dots m} \\ &= \{\Pr[M(k) = M_j | M(k-1) = M_i]\}_{i,j=1,\dots m}\end{aligned} \quad (12)$$

models the dynamical switching among m models, or *modes*, $\{M_j\}_{j=1,\dots,m}$. Each mode evolves independently of the others, but the overall estimate combines the outputs of all modes. Indeed each step of the algorithm is composed of the three phases illustrated in Fig. 2:

i) *Interaction/Mixing*: the *mixing probabilities* $\mu^{i|j}_{k-1|k-1}$, i.e., the probability that mode i was in effect at time $k-1$, if mode j is in effect at time k, conditioned to $\mathbf{y}_{0:k-1}$, are computed according to:

$$\mu^{i|j}_{k-1|k-1} = \frac{p_{ij}\mu^i_{k-1}}{\sum_{i=1}^m p_{ij}\mu^i_{k-1}}, \qquad i,j = 1,\dots,m, \quad (13)$$

where μ^i_{k-1} is the mode probability of node i at the step $k-1$.
For each mode $j = 1,\dots,m$, the *initial state and covariance estimates* are given

$$\widehat{\mathbf{x}}^{0j}_{k-1|k-1} = \sum_{i=1}^m \widehat{\mathbf{x}}^i_{k-1|k-1}\mu^{i|j}_{k-1|k-1}, \quad (14)$$

$$\begin{aligned}\widehat{\mathbf{P}}^{0j}_{k-1|k-1} = \sum_{i=1}^m \Big[\widehat{\mathbf{P}}^i_{k-1|k-1} + \Big(\widehat{\mathbf{x}}^i_{k-1|k-1} - \widehat{\mathbf{x}}^{0j}_{k-1|k-1}\Big) \\ \Big(\widehat{\mathbf{x}}^i_{k-1|k-1} - \widehat{\mathbf{x}}^{0j}_{k-1|k-1}\Big)^T\Big] \mu^{i|j}_{k-1|k-1}\end{aligned} \quad (15)$$

where $\widehat{\mathbf{x}}^i_{k-1|k-1}$ and $\widehat{\mathbf{P}}^i_{k-1|k-1}$ are the estimates yielded by mode i at the previous step.

ii) *Mode-matched filtering*, in which each mode computes the a posteriori estimates $\widehat{\mathbf{x}}^i_{k|k}$ and $\widehat{\mathbf{P}}^i_{k|k}$ and the likelihoods corresponding to the m models, i.e. the quantity

$$\Lambda^j_k = p(\mathbf{y}_k | M_j, \mathbf{y}_{0:k-1}) \quad (16)$$

in which M_j indicates the j-th model.

iii) *Mode probability update*: the new *mode probabilities* μ^j_k are calculated as

$$\mu^j_k = \frac{1}{c}\Lambda^j_k \sum_{i=1}^m p_{ij}\mu^i_{k-1}, \quad (17)$$

where c is a normalizing constant. The IMM estimate is then achieved by weighting the a posteriori estimates by

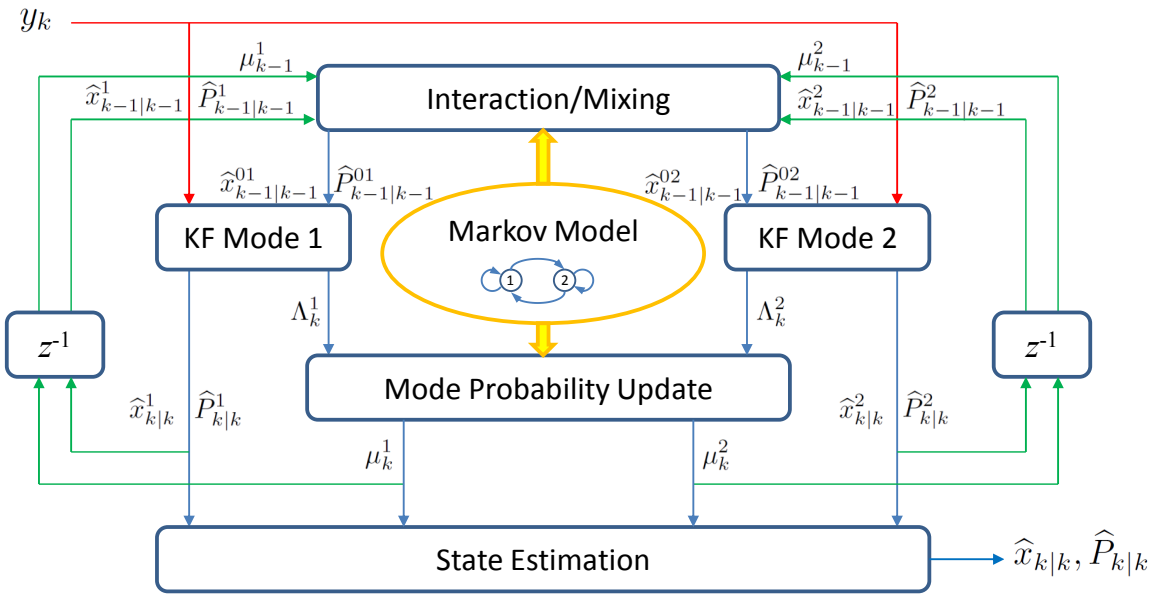

Fig. 2: One step of the IMM estimator with two models.

the mode probabilities:

$$\widehat{\mathbf{x}}_{k|k} = \sum_{i=1}^{m} \widehat{\mathbf{x}}^i_{k|k} \mu^i_k. \tag{18}$$

Accordingly, the design of an IMM algorithm involves the selection of the m modes to mix and the choice of the Markov chain. The latter is characterized by the transition probabilities $\{p_{ij}\}_{i,j=1,\dots m}$ and by the initial probabilities of each mode,

$$\mu^j_0 = \Pr\left(M\left(0\right) = M_j\right), \tag{19}$$

that however do not represent critical parameters of the approach [9].

III. Proposed Algorithms

We now present some relevant details of both methods considered for estimating the htr/HSR sequence $\mathcal{E} = \{\mathbf{E}_k : k \in [0, K]\}$, namely the KF and the IMM, the latter comprising just two KFs (so called *baseline IMM* [23]).

A. State evolution and propagation step

The state equation formalization (1) requires, first of all, the specification of the transition function $\mathbf{f}_k(\cdot)$, or its linear counterpart $\mathbf{A}_k$, and the statistical characterization of the process noise $\mathbf{w}_k$.

In our case, at least in principle, the transitions among states $\mathbf{x}_k$ and $\mathbf{x}_{k-1}$ could be modeled after physical analysis of the temperature dynamics accounting for the incoming solar radiation, the precipitations, the physical features of the surface and other factors, and hence implying correlation of the image sequences in both time and space. For sake of simplicity we assume a linear, albeit time varying, form for $\mathbf{f}_k(\cdot)$:

$$\widehat{\mathbf{x}}_{k|k-1} = \mathbf{A}_k \widehat{\mathbf{x}}_{k-1|k-1} \tag{20}$$

and further neglect the spatial correlation among pixels, that however will be recaptured in the update phase, as detailed later. Accordingly, we assume a diagonal state-transition matrix

$$\mathbf{A}_k = diag\left(a_k(1), \dots, a_k(S)\right) \tag{21}$$

and a diagonal noise *covariance matrix* $\mathbf{Q}_k = \sigma^2_m \mathbf{I}$, for all k. Each entry $a_k(i)$ accounts for the daily time variations of the brightness of pixel i and is estimated by the available information at time k and $k-1$, and in particular as the ratio

$$\widehat{a}_k(i) = \mathcal{B}\left(\frac{\mathbf{L}_k\left(j\left(i\right)\right)}{\mathbf{L}_{k-1}\left(j\left(i\right)\right)}\right), \tag{22}$$

where $j(i)$ is the htr/LSR pixel corresponding to the htr/HSR pixel i, and $\mathcal{B}(\cdot)$ is the bicubic interpolation operator.

Furthermore we assume that the system evolution starts at an instant belonging to T_H, so that the initial state $\hat{x}_{0|0}$ is exactly known. Thus the initial covariance $\mathbf{P}_{0|0} = \mathbf{0}$, namely the null matrix of proper order.

B. Observation model and update step

Since the analysis of this work is restricted to the instants $k \in T_L$ in which the htr/LSR sequence is available and since the support T_H of $\mathcal{H}$ is a subset of T_L, at any time k at least the LR data, but occasionally both the LR and HR data, are available. When the HR image $\mathbf{H}_k$ is accessible, we simply utilize it as observation

$$\mathbf{y}_k = \left[H_k\left(1\right), \dots, H_k\left(S\right)\right]^T. \tag{23}$$

As already pointed out for the system initialization, in this case the htr/HSR image $\mathbf{E}_k$ coincides with the true image, i.e. $\mathbf{E}_k = \mathbf{H}_k$ and thus we put the observation noise covariance to zero

$$\mathbf{R}_k = \mathbf{0}. \tag{24}$$

When only the LR image is accessible, the classical solution adopted in Bayesian methods exploits a physical model between the observation and the state. In particular, simple geometric considerations suggest to define the LR observation as the average, possibly weighted according to the Point Spread Function (PSF) of the LR sensor, of the corresponding HR pixels. However we resort to a cruder approximation that consists in defining $\mathbf{y}_k$ as a HR observation derived from $\mathbf{L}_k$ through a bicubic interpolation operator $\mathcal{B}(\cdot)$, namely as

$$\mathbf{y}_k := \mathrm{vec}(\mathcal{B}(\mathbf{L}_k)) \tag{25}$$

This approach, that we refer to as *Interpolated Observation Model* (*IOM*), has the merit of introducing an implicit spatial dependency among the observation pixels that spans outside the limits of a single LR pixels [1], [3]. The IOM strictly fulfills the Markov hypothesis embedded in the SSM formalization, namely conditional independence of $\mathbf{y}_k$ from the past, given the current value of the state. However the possibility of deriving a more precise observation from the whole sequences L and H

$$\mathbf{y}_k = \eta(\mathcal{L}, \mathcal{H}), \tag{26}$$

deserves further attention. Profiting from the pansharpening experience [6], we construct an enhanced observation $\mathbf{y}_k$ by adding the details extracted from the latest available HR image to the current LR image $\mathbf{L}_k$, namely we define $\mathbf{y}_k$ as

$$\mathbf{y}_k := \mathrm{vec}(\mathcal{S}(\mathbf{H}_{m_k}, \mathcal{B}(\mathbf{L}_k))),\ m_k = \max_{m \in T_H} \{m \leq k\}, \tag{27}$$

where $S(\mathbf{X}, \mathbf{Y})$ is the sharpening operator that uses the HR image $\mathbf{X}$ and the LR image $\mathbf{Y}$. This approach, here called *Sharpened Observation Model* (*SOM*), is based on the hypothesis that the details of the HR TIR image are related to the physical composition of the illuminated surface and thus have a slow variation. The validity of this hypothesis decreases the difference of the actual instant k and the time m_k at which the last HR image was acquired. Accordingly we modify in this work the classical pansharpening scheme by weighting the details injection by a coefficient that accounts for the similarity of $\mathbf{H}_{m_k}$ and $\mathcal{B}(\mathbf{L}_k)$. We employ the *Normalized Cross Correlation Coefficient NCCCoef* [22]

$$\rho(\mathbf{H}_{m_k}, \mathcal{B}(\mathbf{L}_k)) = \frac{\mathbf{H}_{m_k} \cdot \mathcal{B}(\mathbf{L}_k)}{\sqrt{\mathbf{H}_{m_k} \cdot \mathbf{H}_{m_k}} \sqrt{\mathcal{B}(\mathbf{L}_k) \cdot \mathcal{B}(\mathbf{L}_k)}} \tag{28}$$

in which $\mathbf{X} \cdot \mathbf{Y}$ denotes the scalar product of images $\mathbf{X}$ and $\mathbf{Y}$.

IV. Experimental Results

In this Section the results of algorithms' validation procedures is reported. Two different protocols, employing images acquired by a single sensor and a couple of sequences collected by two sensors, respectively, are used for assessing the developed algorithms and are described in the following.

A. Datasets description and implementation issues

We exploit the availability of three different datasets composed of thermal images collected by the SEVIRI sensor (*IR10.8* channel, 10.8 μm) and by the MODIS sensor (band 31, $[10.7811.28]$ μm). All refer to clear sky images in order to preserve the validation procedure from unpredictable corruption effects. In the presence of clouds, the algorithm is preceded by a preliminary phase of cloud masking [2].

The first dataset (henceforth referred to as the *Sardinia dataset*) is composed only of SEVIRI images, acquired on 24 August 2011 in an area of the Sardinia Island (latitude between 39.44 and 40.82 degrees North, longitude between 8.64 and 9.54 degrees East) and projected over a grid of 0.06 degrees.

The other two datasets are composed by both SEVIRI and MODIS images. The *Greece dataset* contains two MODIS images, acquired on 23 August 2011 at 20.25 UTC by Terra satellite and on 24 August 2011 at 00.35 UTC by Aqua satellite, respectively, and of SEVIRI images collected in the same time interval over an area of the Balkan Peninsula (latitude between 39.62 and 42.44 degrees North, longitude between 22.46 and 26.30 degrees East). The sequences have been suitably intercalibrated and coregistered through the projection over a grid of 0.01 degrees. In this test the first MODIS image is used as the starting HR image, and the second as the reference image to estimate.

Finally the *Campania dataset* refers to an area of Southern Italy (latitude from 40.01 to 40.93 degrees North, longitude from 14.09 to 15.48 degrees East), relevant for the irrigation project IRRISAT to which the research group participates [28]. Three MODIS images were collected on 16 June 2013 between 09.25 UTC and 20.30 UTC. They were suitably intercalibrated and coregistered with the corresponding SEVIRI acquisitions by georeferencing and projecting over a grid of 0.01 degrees.

Performance assessment was performed by comparing the proposed Bayesian algorithms, based on the KF and IMM, with the reference non sequential approaches; both the IOM and SOM, described in Sect. III-B have been subject of investigation. Accordingly, we compared the following strategies:

B. Simulated data

- *Nearest-neighbor image estimation* (*N*): the estimate at time k is achieved by simply resampling the LR images through a nearest-neighbor interpolation rule.
- *Interpolated image estimation* (*I*): the estimate at time k is achieved by interpolating the LR images through a bicubic interpolation scheme, namely we define the algorithm output according to Eq. (25).
- *Sharpened image estimation* (*S*): the estimate at time k is achieved by sharpening the interpolated LR image through the injection of the details extracted from the last available HR image, as described by Eq. (27). In particular a modified version of the *High Pass Modulation* (*HPM*) (or *High Frequency Modulation - HFM*) injection scheme [29] is employed due to its remarkable features [5], [34]. In this approach the sharpened image is defined

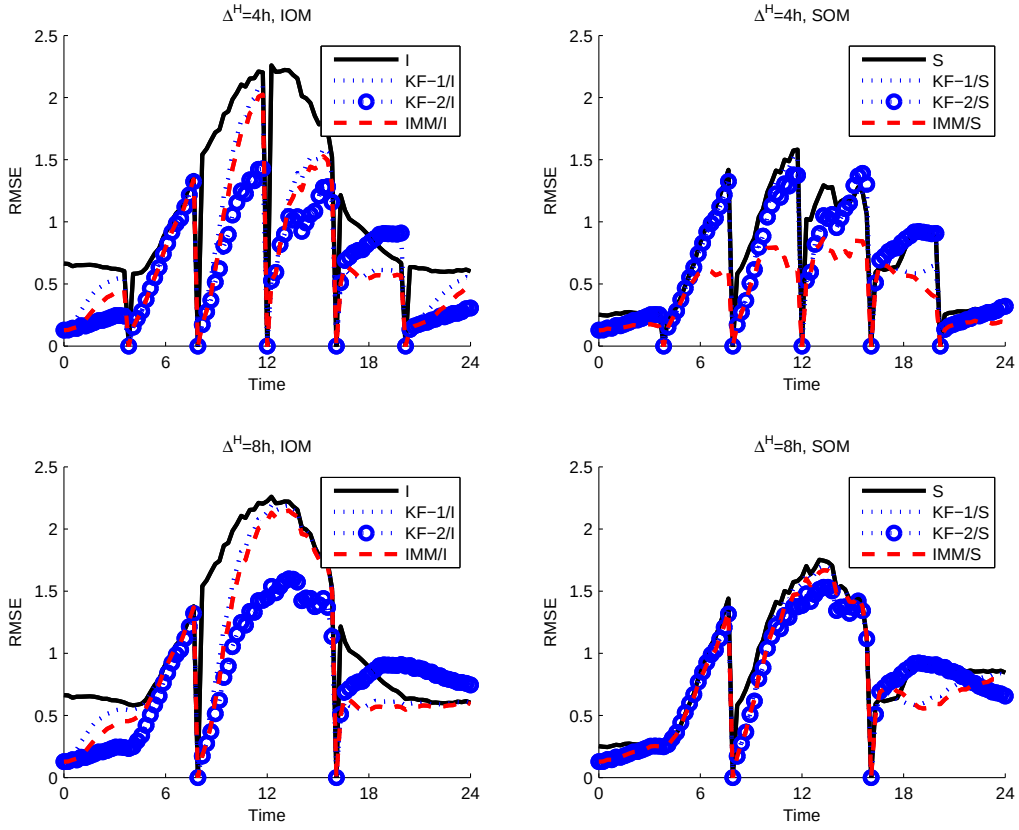

Fig. 3: RMSE computed between the forecast of TIR SEVIRI image and the actual value for the simulated Campania dataset and $\Delta^H = 4$ (top plots) and $\Delta^H = 8$ (bottom plots): IOM (on the left) and SOM (on the right). The KF 1-algorithm works with $\sigma_m = 0.2$, the KF-2 algorithm with $\sigma_m = 0.04$ and both use $\sigma_o = 1$; the IMM employs KF-1 and KF-2 as modes, and the transition probabilities are $p_{12} = p_{21} = 0.1$.

as

$$\mathbf{E}_k = \mathcal{B}(\mathbf{L}_k) + \rho \frac{\mathcal{B}(\mathbf{L}_k)}{\mathbf{H}^{LP}_{m_k}} \left(\mathbf{H}_{m_k} - \mathbf{H}^{LP}_{m_k}\right), \qquad (29)$$

in which $\mathbf{H}^{LP}$ represents a low pass version of the HR image $\mathbf{H}$ and ρ is the NCCCoef, given by (28). In this work we achieve $\mathbf{H}^{LP}$ by a MultiResolution Analysis implemented by the undecimated wavelet decomposition [26]. More in detail we exploit the *undecimated "a' trous"* algorithm [31] carried out by the successive application, by row and columns, of a filter derived from the choice of a B_3 cubic spline as scaling function [32].

- *Kalman Filter with Interpolated observation* (*KF/I*): the Kalman Filter recursion described in Sect. II-A is employed for yielding the desired estimate by utilizing the IOM described in Eq. (25).
- *Kalman Filter with Sharpened observation* (*KF/S*): the Kalman Filter is fed by observations constructed by the SOM paradigm, implemented as in Eq (29).
- *Interacting Multiple Model with Interpolated observation* (*IMM/I*): the estimate is provided from the IMM algorithm detailed in Sect. II-B and operating with the IOM defined in Eq. (25).
  Two models have been used for this work, namely we used $m = 2$. They consist in two KFs with different tracking capabilities. The first is optimized for taking into greater account the propagation phase and turns out to be more useful at the instants that follow the acquisition of the HR image. Indeed in that case it is preferable to let the system spontaneously evolve from the latter, rather than give more credit to the current LR acquisition. On the other side, after some instants the previously acquired HR image does not reflect the actual thermal radiation anymore and thus the present LR observation has to be fully exploited, besides its inaccuracy. The transition between the two regimes happens in different time intervals that shorten when abrupt changes of the thermal dynamics occur (e.g. at the sunrise or at the sunset) and grow in the presence of slow temperature variations (e.g., during the night). The purpose of the IMM algorithm is to follow this behavior, by automatically swapping from the propagation-oriented mode (characterized by a greater standard deviation of the state noise σ_m), to the observation-oriented mode (characterized by a smaller σ_m). The Markov chain employed to this purpose is supposed to be time-space homogeneous (namely, the same values $p_{11} = p_{22} = 0.9$ are used for all pixels and for all time instants). Furthermore the likelihood (16), required for estimating the mode probabilities, are

TABLE I: RMSE related to simulated scenarios for several values of Δ^H. The original images, used as ltr/HSR and GT sequences, have 6 km/pixel resolution, whereas the simulated htr/LSR sequences have 36 km/pixel resolution ($r = 6$). The KF- and IMM-based algorithms work with $\sigma_O = 1$. The RMSE value is achieved by averaging both over space and time, namely over the whole sequence of images.

	Δ^H [h]	N	I	S	KF/I		KF/S		IMM/I	IMM/S
					$\sigma_m = 0.2$	$\sigma_m = 0.04$	$\sigma_m = 0.2$	$\sigma_m = 0.04$	$\sigma_m = \{0.2, 0.04\}$	$\sigma_m = \{0.2, 0.04\}$
Sardinia	1	1.12	1.09	0.50	0.28	0.26	0.26	0.26	0.26	0.26
	2	1.21	1.17	0.61	0.54	0.45	0.45	0.45	0.48	0.44
	4	1.25	1.21	0.76	0.85	0.72	0.68	0.73	0.78	0.68
	8	1.28	1.24	0.89	1.08	0.86	0.87	0.90	1.02	0.85
Campania	1	1.21	1.14	0.53	0.35	0.34	0.34	0.34	0.34	0.34
	2	1.31	1.23	0.65	0.59	0.51	0.50	0.51	0.54	0.50
	4	1.35	1.28	0.83	0.91	0.74	0.73	0.75	0.86	0.72
	8	1.38	1.30	0.99	1.14	0.93	0.93	0.90	1.10	0.91

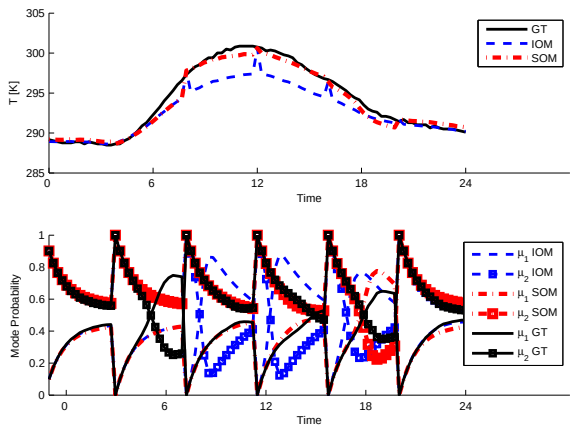

Fig. 4: Brightness Temperatures (top plot) and mode probabilities (bottom plot) for a pixel of the Campania datasets related to the Sele region. The plots corresponding to the actual values (GT) are depicted in black, while blue and red colors refer to the IOM and the SOM, respectively.

obtained by assuming a Gaussian distribution [9]

$$\Lambda_k^j = \mathcal{N}\left(\mathbf{y}_k; \widehat{\mathbf{x}}_{k-1|k-1}^{0j}, \widehat{\mathbf{P}}_{k-1|k-1}^{0j}\right), \qquad (30)$$

in which $\mathcal{N}(\mathbf{y}; \mathbf{x}, \mathbf{P})$ denotes the probability density function of a Normal random variable with mean $\mathbf{x}$ and covariance matrix $\mathbf{P}$, calculated at point $\mathbf{y}$.

- *Interacting Multiple Model and Sharpened observation* (*IMM/S*): this last method consists in employing the IMM algorithm with the same settings specified at the previous item, but fed the images sharpened through Eq. (29).

We firstly employ the simulated datasets in that they offer a perfectly controlled scenario. The original SEVIRI sequence, characterized by a sampling interval $\Delta^L = 15$ minutes, is used as htr/HSR sequence, from which we extract a subset of images, with variable interval $\Delta^H = \{1, 2, 4, 8\}$ hours, representing the ltr/HSR sequence. The htr/LSR is simulated by averaging the contribution of HR pixels within contiguous non overlapping cells. Several resolution ratios r between the HR and the LR images have been used for assessing the performances of the method, but we report in this paper the results achieved for $r = 6$ that is directly comparable with real data analysis reported below, namely with the actual resolution ratio existing between the SEVIRI and MODIS sensors. The performances of the employed Kalman Filters depend on the state and measurement standard deviations σ_m and σ_o, and in particular on their ratio σ_m/σ_o. Accordingly we set the observation std to $\sigma_o = 1$ and, after a preliminary tuning phase, the state standard deviations to: $\sigma_m = 0.2$ and $\sigma_m = 0.04$. The two corresponding KFs, named KF-1 (for $\sigma_m = 0.2$) and KF-2 (for $\sigma_m = 0.04$), privilege the update and the propagation step, respectively.

The performances have been evaluated in terms of the *Root Mean Square Error* (*RMSE*) calculated on the zones of the images corresponding to the land. In this simulated case the RMSE can be computed at each instant, being all the reference images available. The RMSE plot Vs. time is shown in Fig. 3 and refers to the Campania dataset with a ltr/HSR sampling rate of $\Delta^H = 4$ (top plots) and $\Delta^H = 8$ (bottom plots), while the overall values, calculated by averaging, over the whole sequence, the RMSE corresponding to each image are reported in Tab. I for the Sardinia and the Campania datasets.

The behavior of the different algorithms in Fig. 3 reflects the dynamics of the BT during daytime that is particularly fast at the sunrise, when the incoming radiation causes a sudden increase of the temperature.

The first remarkable result, more evident in the case of $\Delta^H = 4$, in which the past observations constitute a more significant aid for building the current estimate, concerns the usefulness of the sequential Bayesian methods. As expected, for both values of Δ^H, in the presence of a less accurate LR information (namely with IOM), the KF-2 filter achieves better performances with respect to KF-1, since it preserves the benefits of the HR acquisitions for a greater amount of time; in other terms, this setting highlights the contribution of the sequential filtering approach, with respect to memoryless techniques. The behavior of the IMM method is here not particularly satisfactory, since its performances are in between the values obtained by the two KFs.

On the other side, application of the SOM allows to achieve, in most cases, better performances, though flattening the differences between the tracking methods, especially for $\Delta^H = 8$.

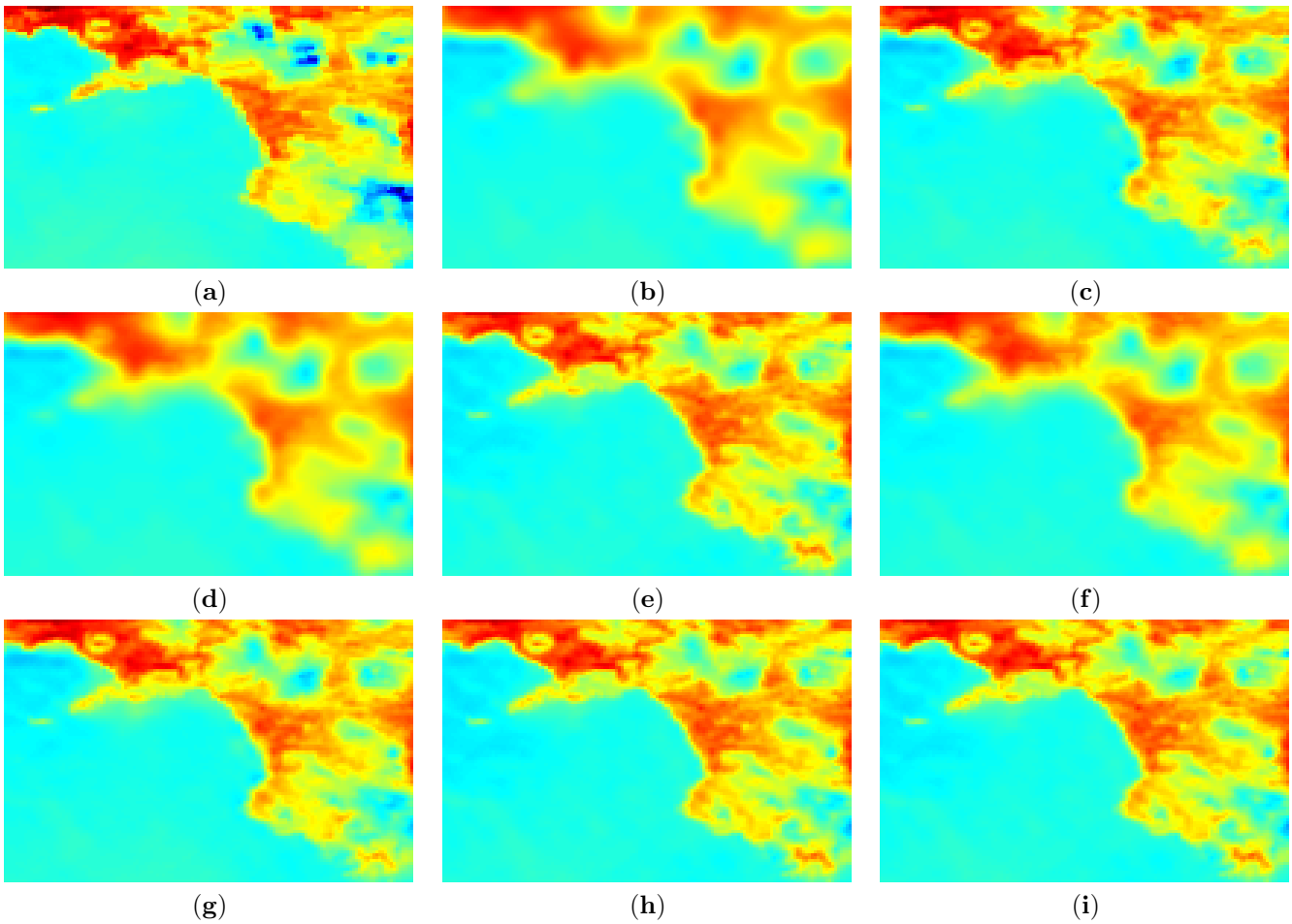

Fig. 5: Campania dataset, acquired on 16 June 2013 between 09.25 UTC and 12.45 UTC. The reference image is reported in subplot (a); The outputs of estimation procedures, operating with the same parameters as in Fig. (3), in the subplots: (b) static IOM algorithm; (c) static SOM algorithm; (d) KF-1/I; (e) KF-2/I; (f) IMM/I; (g) KF-1/S; (h) KF-2/S; (i) IMM/S.

This is due to the higher quality of the observation that can be deduced both by the plot of the RMSE versus time reported in black solid line in Fig. 3 and by the exemplary BT trend of a single pixel, depicted in the top plot of Fig. 4. The greater accuracy reflects also in a more proper functioning of the IMM models switch, as testified by the bottom plot of Fig. 4, containing the values of the mode probabilities μ_1 and μ_2. It is evident that with SOM the IMM mixes its state almost as with the actual observation. This yields a smaller RMSE that can be observed in the right plots of Fig. 3, as well as by reading the values reported in Tab. I. Also in this case, the effects of the tracking procedures decreases with the growth of the sampling interval Δ^H.

C. Real data

The second validation procedure exploits the two real datasets of SEVIRI and MODIS acquisitions over the Balkan Peninsula and the Southern Italy. The spatial resolution ratio is $r = 6$, that was chosen also in the simulated cases to allow for the comparison between the two assessment protocols.

Due to the cited reinitialization procedure performed at each time the HR image is available, a run of the algorithm simply involves the interval between two MODIS images; the latter represents the starting point and the estimation target, respectively, and further observations are constituted by all the SEVIRI images acquired during the same interval. One example regarding the Greece dataset and two examples from Campania dataset have been used to represent different phases of the days and difference lengths of the observation interval.

The assessment results have been collected in Tab. II and show the RMSE calculated on the single available ground truth image, acquired at the end of the working interval. In fact, the reported RMSE values are not directly comparable with those achievable in the practical application of the algorithms, that are intended for yielding an estimate of the missing information at the instants strictly contained between the interval extremes. In a sense, the study reported here represents a worst case analysis of the performances, that most properly helps in setting the limits of the maximum estimation interval length. Thus the most significant remarks derives from comparing the results for different values of Δ^H. Results of the first Campania dataset (see also Fig. 5), acquired between 09.25 UTC and 12.45 UTC, confirm many indications achieved by simulated data analysis. In particular, besides the

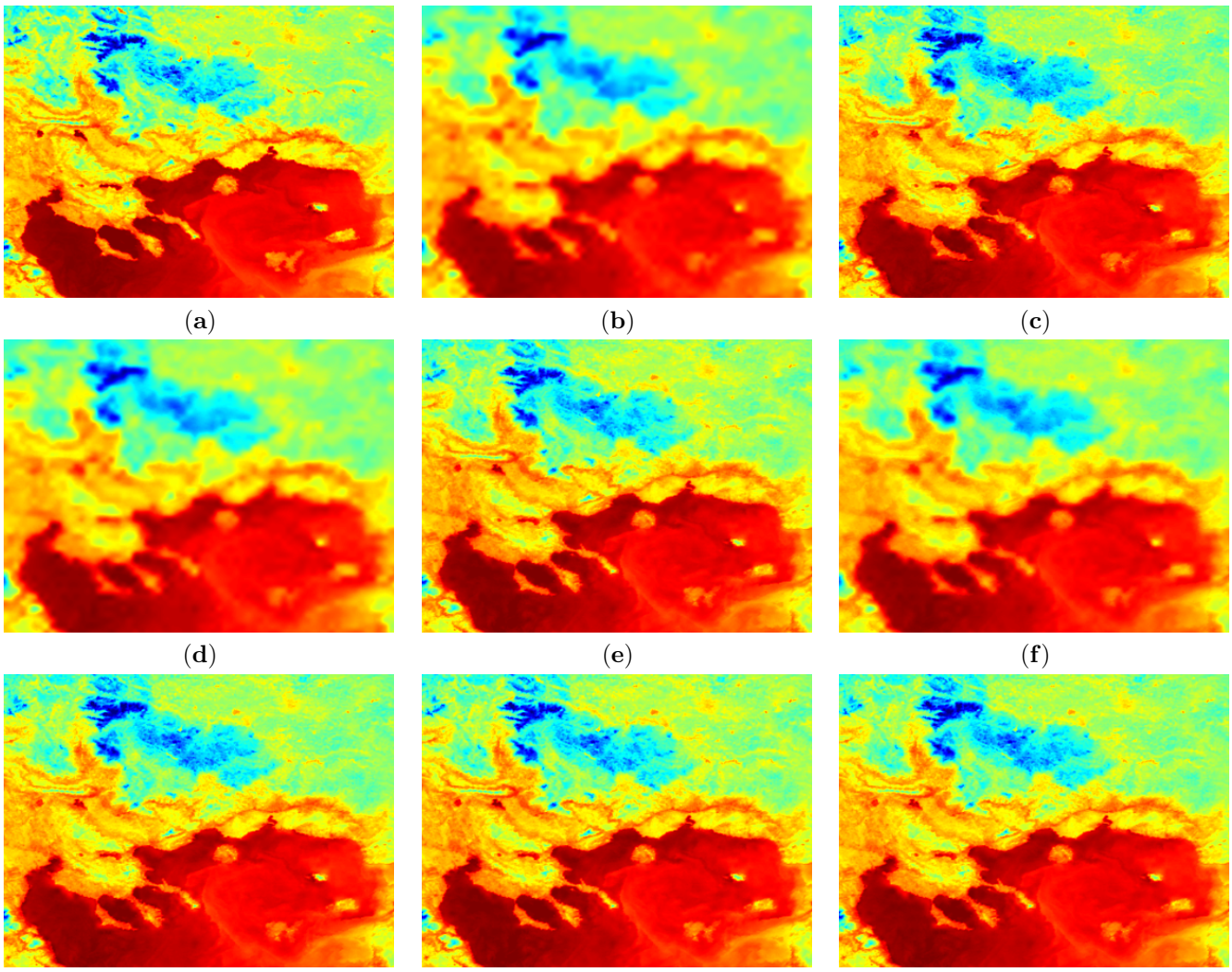

Fig. 6: Greece dataset, acquired between 23 August 2011 at 20.25 UTC and 24 August 2011 at 00.35 UTC. The reference image is reported in subplot (a); The outputs of estimation procedures, operating with the same parameters as in Fig. (3), in the subplots: (b) static IOM algorithm; (c) static SOM algorithm; (d) KF-1/I; (e) KF-2/I; (f) IMM/I; (g) KF-1/S; (h) KF-2/S; (i) IMM/S.

high estimation error values originated by the critical daytime period (see also Fig. 3), the suitability of employing an IMM-based Bayesian procedure with SOM can be evidenced. On the other side, the application of algorithms to the Greece dataset acquired between 20.25 UTC and 00.35 UTC (see Fig. 6) and to the second Campania dataset acquired between 12.45 UTC and 20.30 UTC, yields very different results. Specifically, in the first case only the advantage of propagating the information coming from the first initial MODIS image can be reported, as testified by the best results reached by the KF-2 algorithm. Moreover, the proposed sequential Bayesian procedure may not be appropriate if high accuracy is desired throughout a long interval (e.g., around 8 hours, as in our test case) since, as the distance from the last HR image increases, it does not outperform even a simple interpolation procedure. This behavior matches the general results shown in Fig. 3 for the simulation runs. More specifically, we report in Fig. 7 the RMSE curves achieved through the simulation protocol described in Sect. IV-B on the same time interval, namely by employing the SEVIRI images acquired on the Campania area on 16 June 2013 between 12.45 UTC and 20.30 UTC. The plots illustrate how the effect of propagating the information extracted by the initial HR image decreases over time and is completely lost after 8 h; on the other side, the robustness of the proposed IMM approach is further evidenced, being able to achieve remarkable performances during the whole considered interval.

V. Conclusions

In this work a technique for fusing thermal images, acquired by sensors with different temporal and spatial resolutions, is proposed. It relies upon the Sequential Bayesian estimation framework, and specifically has been implemented in two versions: the classical Kalman Filter and the Interacting

TABLE II: RMSE related to real data scenarios. The spatial resolution of the MODIS ltr/HSR sequence is 1 km/pixel, whereas that of the SEVIRI htr/LSR sequences is 6 km/pixel ($r = 6$). The KF- and IMM-based algorithms work with $\sigma_O = 1$. The RMSE is achieved by averaging only over space, namely over the unique reference image.

	Δ^H [h]	N	I	S	KF/I		KF/S		IMM/I	IMM/S
					$\sigma_m = 0.2$	$\sigma_m = 0.04$	$\sigma_m = 0.2$	$\sigma_m = 0.04$	$\sigma_m = \{0.2, 0.04\}$	$\sigma_m = \{0.2, 0.04\}$
Greece	4	0.85	0.79	0.62	0.74	0.48	0.60	0.50	0.69	0.57
Campania	3	1.67	1.50	1.32	1.41	1.27	1.28	1.28	1.36	1.25
	8	0.64	0.61	0.73	0.61	0.92	0.65	0.94	0.60	0.62

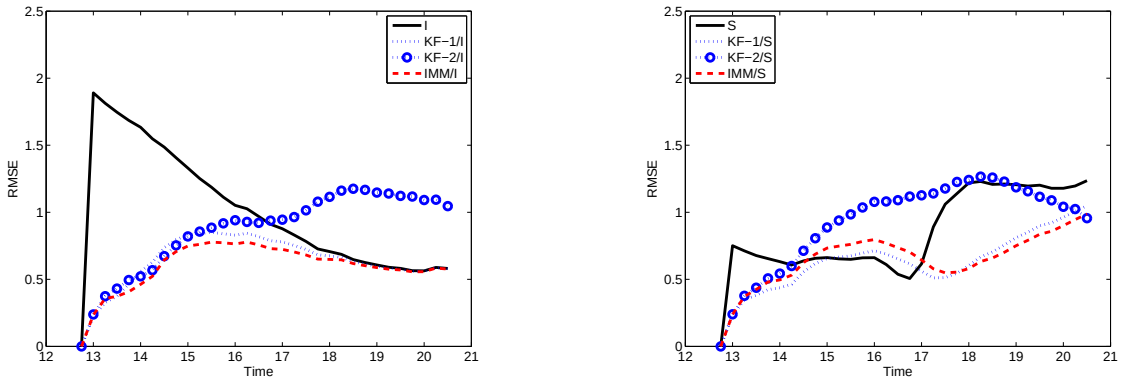

Fig. 7: RMSE computed between the forecast of TIR SEVIRI image and the actual value for the simulated Campania dataset related to the time interval between 12.45 UTC and 20.30 UTC on 16 June 2013: IOM (on the left) and SOM (on the right). The KF 1-algorithm works with $\sigma_m = 0.2$, the KF-2 algorithm with $\sigma_m = 0.04$ and both use $\sigma_o = 1$; the IMM employs KF-1 and KF-2 as modes, and the transition probabilities are $p_{12} = p_{21} = 0.1$.

Multiple Model paradigms. The latter allows to overcome the difficulties introduced by the different operational regimes that the estimation algorithm copes with during the different phases of the day (and of the year). In addition a static sharpening procedure, useful also for preparing the inputs of the sequential algorithms, is here developed by analogy with the pansharpening applications. All the developed techniques have been assessed by means of real data acquired by the SEVIRI and MODIS sensors.

Current studies concern the usage of the proposed approaches for agricultural applications. In particular, some particular topics, as irrigation management, do not require real time functioning, and thus the most significant issue raised by this work, namely the applicability of the proposed technique for long estimation intervals, can be faced by exploiting the information acquired also after the estimation instant. In this case, more effective Bayesian procedure, named smoothing algorithms, can be utilized instead of the filtering techniques employed here. This different class of methods constitutes the main research line moving from this study.

ACKNOWLEDGMENTS

The authors thank Dr. P.G. Marchetti and the Service Support and Ground Segment Technology Section at ESA-ESRIN, Frascati (Italy) for providing the SEVIRI data, and acknowledge NASA LAADS web for providing the MODIS data.

REFERENCES

[1] P. Addesso, , M. Longo, R. Restaino, and G. Vivone. Enhancing TIR image resolution via interacting sequential Bayesian estimation. In *IEEE Geoscience and Remote Sensing Symposium (IGARSS), 21-26 July, Melbourne, Australia*, pages 3108–3111, 2013.

[2] P. Addesso, R. Conte, M. Longo, R. Restaino, and G. Vivone. MAP-MRF cloud detection based on PHD filtering. *IEEE J. Sel. Topics Appl. Earth Observ.*, 5(3):919–929, June 2012.

[3] P. Addesso, R. Conte, M. Longo, R. Restaino, and G. Vivone. A sequential bayesian procedure for integrating heterogeneous remotely sensed data for irrigation management. In *Proc. SPIE Remote Sensing*, number 8531, pages 85310C–1 – 85310C–10, 2012.

[4] N. Agam, W.P. Kustas, M.C. Anderson, F. Li, and C.M.U. Neale. A vegetation index based technique for spatial sharpening of thermal imagery. *Remote Sens. Environ.*, 107(4):545–558, Apr. 2007.

[5] B. Aiazzi, L. Alparone, S. Baronti, I. Pippi, and M. Selva. Generalised laplacian pyramid-based fusion of MS + P image data with spectral distortion minimisation. *ISPRS Internat. Archives Photogramm. Remote Sensing*, 34(3A-W3):3–6, 2002.

[6] I. Amro, J. Mateos, M. Vega, R. Molina, and A.K. Katsaggelos. A survey of classical methods and new trends in pansharpening of multispectral images. *EURASIP J. Adv. Sig. Pr.*, 79:1–22, Sep. 2011.

[7] MC Anderson, WP Kustas, JM Norman, CR Hain, JR Mecikalski, L Schultz, MP Gonzalez-Dugo, C Cammalleri, G d'Urso, A Pimstein, et al. Mapping daily evapotranspiration at field to continental scales using geostationary and polar orbiting satellite imagery. *Hydrol. Earth Syst. Sci.*, 15(1):223–239, 2011.

[8] MC Anderson, JM Norman, WP Kustas, R Houborg, PJ Starks, and N Agam. A thermal-based remote sensing technique for routine mapping of land-surface carbon, water and energy fluxes from field to regional scales. *Remote Sens. Environ.*, 112(12):4227–4241, 2008.

[9] Y. Bar-Shalom, X.R. Li, and T. Kirubarajan. *Estimation with Applications to Tracking and Navigation: Theory Algorithms and Software*. John Wiley And Sons, 2001.

[10] H.A.P. Blom and Y. Bar-Shalom. The interacting multiple model algorithm for systems with markovian switching coefficients. *IEEE Trans. Autom. Control*, 33(8):780–783, 1998.

[11] D. Fasbender. Bayesian data fusion for adaptable image pansharpening. *IEEE Trans. Geosci. and Remote Sens.*, 46(6):1847–1857, Jun. 2008.

[12] F. Gao, J. Masek, M. Schwaller, and F. Hall. On the blending of the landsat and MODIS surface reflectance: predicting daily Landsat surface reflectance. *IEEE Trans. Geosci. Remote Sens.*, 44(8):2207–2218, Aug. 2006.

[13] Z. Ghahramani. An introduction to Hidden Markov Models and Bayesian networks. *Int. J. Pattern Recogn.*, 15(1):9–42, 2001.

[14] L. Giglio, J. Descloitres, C. O. Justice, and Y. J. Kaufman. An enhanced contextual fire detection algorithm for modis. *Remote Sens. Environ.*, 87(2):273–282, 2003.

[15] P.R Houser, G.J.M. De Lannoy, and J.P. Walker. Land surface data assimilation. In W. Lahoz, B. Khattatov, and R. Ménard, editors, *Data Assimilation. Making Sense of Observations*, pages 549–597. Academic Press, 2010.

[16] P.L. Houtekamer and H.L. Mitchell. Data assimilation using an ensemble Kalman filter technique. *Mon. Wea. Rev.*, 126(3):796–811, Mar. 1998.

[17] B. Huang and H. Song. Spatiotemporal reflectance fusion via sparse representation. *IEEE Trans. Geosci. Remote Sens.*, 50(10):3707–3716, Oct. 2012.

[18] R.E. Kalman. A new approach to linear filtering and prediction problems. *J. Basic Eng.-T ASME*, 82(1):35–45, 1960.

[19] W.P. Kustas, J.M. Norman, M.C. Anderson, and A.N. French. Estimating subpixel surface temperatures and energy fluxes from the vegetation indexradiometric temperature relationship. *Remote Sens. Environ.*, 85(4):429–440, Jun. 2003.

[20] F. Laporterie-Déjean, H. de Boissezon, G. Flouzat, and M.-J. Lefèvre-Fonollosa. Thematic and statistical evaluations of five panchromatic/multispectral fusion methods on simulated PLEIADES-HR images. *Inform. Fusion*, 6(3):193–212, 2005.

[21] X.R. Li and V.P. Jilkov. Survey of maneuvering target tracking. part v: Multiple-model methods. *IEEE Trans. Aerosp. Electron. Syst.*, 41(4):1255–1178, Oct. 2005.

[22] J. Marcello, F. Eugenio, and F. Marques. Cloud motion estimation in SEVIRI image sequences. In *Proc. of IEEE Geoscience and Remote Sensing Symposium (IGARSS)*, volume 3, pages 642–645, 2009.

[23] E. Mazor, A. Averbuch, Y. Bar-Shalom, and J. Dayan. Interacting multiple model methods in target tracking: a survey. *IEEE Trans. Aerosp. Electron. Syst.*, 34(1):103–123, 1998.

[24] Ali Mohammadzadeh, Ahad Tavakoli, Valadan Zoej, and J Mohammad. Road extraction based on fuzzy logic and mathematical morphology from pan-sharpened ikonos images. *Photogramm. Rec.*, 21(113):44–60, 2006.

[25] J. Nichol. An emissivity modulation method for spatial enhancement of thermal satellite images in urban heat island analysis. *Photogramm. Eng. Rem. Sens.*, 75(5):1–10, May 2009.

[26] J. Nunez, X. Otazu, O. Fors, A. Prades, V. Pala, and R. Arbiol. Multiresolution-based image fusion with additive wavelet decomposition. *IEEE Trans. Geosci. Remote Sens.*, 37(3):1204–1211, May 1999.

[27] E. Pardo-Igúzquiza, M. Chica-Olmo, and P.M. Atkinson. Downscaling cokriging for image sharpening. *Remote Sens. Environ.*, 102(1-2):86–98, May 2006.

[28] IRRISAT Project. Pilotaggio dell'irrigazione a scala aziendale e consortile assistito da satellite, http://www.irrisat.it, 2011.

[29] R.A. Schowengerdt. *Remote Sensing: Models and Methods for Image Processing, 3rd Ed.* Elsevier, 2007.

[30] C. Souza Jr, L. Firestone, L. M. Silva, and D. Roberts. Mapping forest degradation in the eastern Amazon from SPOT 4 through spectral mixture models. *Remote Sens. Environ.*, 87(4):494–506, 2003.

[31] J.-L. Starck, J. Fadili, and F. Murtagh. The undecimated wavelet decomposition and its reconstruction. *IEEE Trans. Image Process.*, 16(2):297–309, Feb. 2007.

[32] G Strang and T. Nguyen. *Wavelets and Filter Banks, 2nd Ed.* Wellesley Cambridge Press, 1996.

[33] H.L. Van Trees. *Detection, Estimation and Modulation Theory, Part I. Detection, Estimation and Linear Modulation Theory*. John Wiley & Sons, 2001.

[34] G. Vivone, R. Restaino, M. Dalla Mura, G. Licciardi, and J. Chanussot. Contrast and error-based fusion schemes for multispectral image pansharpening. *IEEE Geosci. and Remote Sens. Letters,*, 11(5):930–934, May 2014.

[35] C.K. Wikle and L.M. Berliner. A Bayesian tutorial for data assimilation. *Physica D*, 230(1-2):1–16, Jun. 2007.

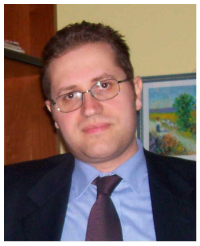

Paolo Addesso received the Laurea degree in electronic engineering (cum laude) and the Ph.D. degree in information engineering both from University of Salerno, Fisciano, Italy, in 2000 and 2005, respectively. He is currently a Research Fellow with the University of Salerno. His main research interests include detection and estimation theory, signal processing, internet traffic modeling, wireless communications, multiterminal inference and sensor networks, statistical characterization of nonlinear devices, gravitational waves detection, fractal models for natural surfaces and remote sensing.

Maurizio Longo (M'14) (MSEE, Stanford, 1977; Laurea in Electronic Eng., 1972, University of Napoli) is Full Professor of Telecommunications at the University of Salerno (Italy), where he also serves as the Chairman of the Committee for Patents and the Director of the Coritel (Consortium for Researches in Telecommunications) Laboratory, having previously served as the Dean of the Dept. of Information Eng. and Electrical Eng. and as the Chairman of the Graduate School of Information Eng. Currently he is member of the Steering Committee of Reslehm (Remote Sensing Lab. for Environmental Hazards Monitoring) and of the Board of Trustees of Coritel. He also held academic positions at the Universities "Federico II" and "Parthenope" in Napoli, the University of Lecce and the Aeronautical Academy. During 1986-87 and in 1990 he was on leave at Stanford University, as a Formez Fellow and as a NATO-CNR Senior Fellow. He is author of over 140 papers, mainly in the in the fields of telecommunication networks and statistical signal processing, the latter with applications to radar, remote sensing and astrophysical observation.

Rocco Restaino (M'14) received the Laurea degree in electronic engineering from the University of Naples, Naples, Italy, in 1998, and the Ph.D. degree in information engineering from the University of Salerno, Fisciano, Italy, in 2002. He is currently an Assistant Professor at the University of Salerno. His research interests include probability theory, stochastic geometry and signal processing for remote sensing and networking.

Gemine Vivone received the B.Sc. (cum laude), the M.Sc. (cum laude) and the Ph.D. degrees in information engineering from the University of Salerno, Italy, in 2008, 2011 and 2014, respectively. He is currently a Research Fellow at the NATO STO Centre for Maritime Research and Experimentation, La Spezia, Italy. In 2013, he was a visiting scholar at the Grenoble Institute of Technology (INPG), Grenoble, France, where he conducted his research at the Laboratoire Grenoblois de l'Image, de la Parole, du Signal et de l'Automatique (GIPSA-Lab). In 2012, he was at the NATO Undersea Research Centre, La Spezia, Italy, as a visiting researcher. His main research interests focus on statistical signal processing, classification of remotely sensed images, data fusion and tracking algorithms.